A Combined FEM/MoM Approach to Analyze the Plane Wave Diffraction by Arbitrary Gratings

Stephen D. Gedney, *Member, IEEE,* Jin Fa Lee, *Member, IEEE,* and Raj Mittra, *Fellow, IEEE*

Abstract—**The diffraction of TE- and TM-polarized plane waves by planar gratings is numerically analyzed using a combined FEM/MoM algorithm based on the generalized network formulation. The interior region, treated using the FEM, is truncated to a single unit cell with the introduction of an exact periodic boundary condition, which is enforced as a natural boundary condition. By employing the finite element method to compute the fields within the periodic structure, gratings of arbitrary cross section and material composition can be efficiently modeled.**

I. Introduction

GRATINGS have found a plethora of applications in many areas of physics and engineering. Some important applications include: microwave lenses and polarizers, twist reflector antennas, spectrum analyzers, integrated optical devices, holography, and acoustooptical devices. Because of their wide usage, the diffraction properties of gratings have been studied extensively over the last few decades (see [1] and [2] for extensive bibliographies). A number of analytical and numerical methods (both approximate and rigorous) have been used to study gratings of various compositions. Analytical methods can only be applied to a limited class of problems, and much emphasis has been put on numerical methods. The coupled-wave approach [3] and the coupled-mode [4] approach have been used to study dielectric gratings. Extensions of these methods have been used to study coated, perfectly conducting gratings [5]. Integral equation methods have also been used to study conducting transmission and reflection gratings [6], [7]. Other rigorous methods such as the modified residue calculus technique [8], [9] have also been used extensively to treat perfectly conducting gratings for a number of applications. More recently, the FEM has been used to treat gratings composed of thick conductors [10], and thick conductors embedded in an inhomogeneous slab [11], [12]. The advantage of using the FEM is that inhomogeneous dielectric or magnetic materials, as well as conductors of arbitrary cross-section can easily be modeled. However, the analyses presented in [11] and [12] were limited to gratings composed of perfect conductors embedded in an inhomogeneous slab, where it was assumed that the maximum profile of the periodic conductors was in a constant plane and that the material medium above or below the conductors was homogeneous.

It is the intent of this paper to study gratings that are composed mostly, or entirely, of penetrable materials using a combined FEM/MoM algorithm based on the generalized network formulation [12], [13]. With the use of equivalent currents, the problem domain is divided into three regions: 1 and 2) the exterior homogeneous regions above and below the grating, and 3) the inhomogeneous interior region. The fields in the exterior region are formulated using the method of moments. In the interior region, the fields perturbed by the equivalent currents are computed using the FEM. In order to truncate this region such that it can be modeled using finite elements, an exact periodic boundary condition is introduced. This boundary condition is enforced as a natural boundary condition, and preserves the sparsity of the finite element matrix. The method provided herein is more robust than the methods presented in [11], [12], and is capable of treating a much larger class of grating problems.

II. General Formulation

The grating to be studied is assumed to be planar (i.e., the dimension of periodicity is along a Cartesian coordinate axis), composed of isotropic dielectric or magnetic materials (lossless or lossy), and it also may have conducting materials embedded within it (see Fig. 1). The material profile is assumed to be inhomogeneous in the region contained between the $y = 0$ and the $y = -d$ planes. Above the $y = 0$ plane, the medium is homogeneous with material constants (ϵ_A, μ_A), and similarly, below the $y = -d$ plane, the medium is homogeneous with material constants (ϵ_B, μ_B). In addition, the profile of the grating is considered invariant along the longitudinal z-direction. Therefore, if the grating is illuminated by a monochromatic plane wave which has no z-variation, the TE- and TM-polarized fields completely decouple and can be treated independently.

This problem is analyzed numerically using the generalized network formulation, [12], [13]. The problem space is divided into three regions: the homogeneous half-spaces

Manuscript received May 14, 1991, revised October 1, 1991.

S. D. Gedney is with the Department of Electrical Engineering, University of Kentucky, Lexington, KY 40506-0046.

J. F. Lee is with the Department of Electrical Engineering, Worcester Polytechnic Institute, Worcester, MA 01609.

R. Mittra is with the Electromagnetics Laboratory, Department of Electrical and Computer Engineering, University of Illinois at Urbana-Champaign, 1406 W. Green Street, Urbana, IL 61801-2991.

IEEE Log Number 9105248.

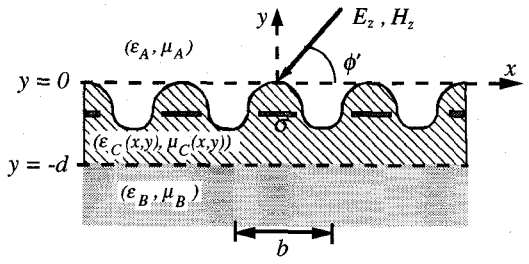

Fig. 1. Inhomogeneous material grating of unit cell width b illuminated by a TE- or TM-polarized monochromatic plane wave.

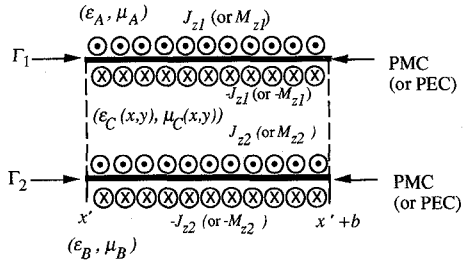

Fig. 2. Equivalent currents J_z (for TM-polarized fields) or M_z (for TE-polarized fields) placed above and below the $y = 0$ and the $y = -d$ planes; shown here for a single unit cell of the grating.

$y > 0$, forming region A; $y < -d$, forming region B; and the interior region C, which contains the periodic structure. The three regions are decoupled by the introduction of equivalent currents which are periodically distributed along x in the $y = 0$ (Γ_1) and the $y = -d$ (Γ_2) planes, as illustrated in Fig. 2. Subsequently, these planes are replaced by PMC (for TM polarization) or PEC (for TE polarization) planes.

If the grating is illuminated by a TM-polarized plane wave, the total electric field in the exterior regions can be expressed as

$$E_z^{\text{tot}} = E_z^{sc} + E_z^{\text{scat}} \tag{1}$$

where E_z^{sc} is the short-circuited electric field due to the PMC plane (i.e., a superposition of the incident field and the specular reflection), and E_z^{scat} is the scattered field produced by the periodic equivalent currents. To enforce the continuity of the electric field across the Γ_1 and the Γ_2 planes, E_z^{tot} is treated as the electric field induced in the interior region when it is excited by the equivalent current sources. In the interior region, the field in the aperture plane is expressed as

$$\begin{aligned} E_{z1}^{\text{tot}} &= E_{z1}^{\text{tot}}(-J_{z1}) + E_{z1}^{\text{tot}}(+J_{z2}) \text{: on } \Gamma_1 \\ E_{z2}^{\text{tot}} &= E_{z2}^{\text{tot}}(+J_{z2}) + E_{z2}^{\text{tot}}(-J_{z1}) \text{: on } \Gamma_2. \end{aligned} \tag{2}$$

The electric field is then matched across the aperture planes into the exterior region, resulting in

$$\begin{aligned} E_z^{sc} &= -E_z^{\text{scat}}(+J_{z1}) + E_{z1}^{\text{tot}}(-J_{z1}) + E_{z1}^{\text{tot}}(+J_{z2}) \text{: on } \Gamma_1 \\ E_z^{sc} &= -E_z^{\text{scat}}(-J_{z2}) + E_{z2}^{\text{tot}}(+J_{z2}) + E_{z2}^{\text{tot}}(-J_{z1}) \text{: on } \Gamma_2. \end{aligned} \tag{3}$$

Floquet's theorem states that given a plane wave incident on a periodic structure, all observable quantities will have the same periodicity as the structure and will also have a cell-to-cell phase shift equivalent to that of periodic structure. This phase shift can be expressed as

$$J_z(x + mb) = J_z(x)\, e^{jk_x mb} \tag{4}$$

where k_x is the x-component of the incident field ($k_x = k \cos \phi'$) and b is the unit cell width. As a result, the fields in (3) can be uniquely described by their distribution over a single unit cell.

The solution of (3) is then obtained using the method of moments. To this end, the equivalent currents J_{z1} and J_{z2} are expanded into a series of basis functions weighted by unknown constant coefficients. Within a unit cell of the structure, the approximate currents are expressed as

$$J_{z1}(x) = \sum_{n=1}^{N} \kappa_n B_n(x); \quad J_{z2}(x) = \sum_{p=1}^{P} \kappa_p B_p(x). \tag{5}$$

A matrix expression is then derived through the inner product of the functionals in (3), expressed as a function of the approximate currents, and a set of testing functions T_k (on Γ_1) and T_q (on Γ_2). Making use of the linearity of the operators, this inner product can be expressed as

$$\begin{bmatrix} E_{zk}^{sc} \\ E_{zq}^{sc} \end{bmatrix} = \begin{bmatrix} [Z^A] & 0 \\ 0 & [Z^B] \end{bmatrix} \begin{bmatrix} \kappa_n \\ \kappa_p \end{bmatrix} + [Z^C] \begin{bmatrix} \kappa_n \\ \kappa_p \end{bmatrix} \tag{6}$$

where the matrix blocks $[Z^A]$ and $[Z^B]$ represent the exterior and $[Z^C]$ represents the interior impedance matrices of the surfaces Γ_1 and Γ_2 over a unit cell. For the TE-polarized case, a dual expression can be derived

$$\begin{bmatrix} H_{zk}^{sc} \\ H_{zq}^{sc} \end{bmatrix} = \begin{bmatrix} [Y^A] & 0 \\ 0 & [Y^B] \end{bmatrix} \begin{bmatrix} \kappa_n \\ \kappa_p \end{bmatrix} + [Y^C] \begin{bmatrix} \kappa_n \\ \kappa_p \end{bmatrix} \tag{7}$$

where $[Y^A]$ and $[Y^B]$ represent the exterior and $[Y^C]$ represents the interior admittance matrices of the surfaces Γ_1 and Γ_2 over a unit cell.

III. Constructing the Exterior Impedance (Admittance) Matrices

The exterior impedance matrices $[Z^A]$ and $[Z^B]$ (or the exterior admittance matrices $[Y^A]$ and $[Y^B]$) are constructed through the inner product of the approximate scattered field with the set of testing functions. The scattered field can be expressed as a superposition of the fields produced by the periodic distribution of equivalent currents. Therefore, using (4)

$$E_z^{\text{scat}}(x, y) = -jk\eta \sum_{m=-\infty}^{\infty} \int_{x=-b/2}^{b/2} 2J_z(x')\, e^{jk_x mb}\, \frac{1}{4j} H_o^{(2)} \cdot (k\sqrt{(x - x' - mb)^2 + (y - y')^2})\, dx'. \tag{8}$$

From Poisson's theorem [14], it can be shown that

$$\sum_{m=-\infty}^{\infty} e^{jk_x mb} \frac{1}{4j} H_o^{(2)}(k|(x - x' - mb)|) = \frac{1}{b} \sum_{m=-\infty}^{\infty} \frac{1}{2j\beta_{ym}} e^{j\beta_{xm}(x-x')} \tag{9}$$

where

$$\beta_{xm} = \frac{2\pi m}{b} + k_x \tag{10}$$

and

$$\beta_{ym} = \begin{cases} \sqrt{k^2 - \beta_{xm}^2}, & (k^2 > \beta_{xm}^2) \\ -j\sqrt{\beta_{xm}^2 - k^2}, & (k^2 < \beta_{xm}^2) \end{cases}. \tag{11}$$

Using (9)–(11), (8) can then be expressed as

$$E_z^{\text{scat}}(x) = \frac{-jk\eta}{b} \sum_{m=-\infty}^{\infty} \tilde{J}_z(\beta_{xm}) \frac{1}{j\beta_{ym}} e^{j\beta_{xm}x} \tag{12}$$

where $\tilde{J}_z(\beta_{xm})$ is the Fourier transform of $J_z(x)$, and $y = y'$.

The equivalent current is expanded into a set of triangle functions, as in (5). The nth basis function centered about $x = x_n$ is expressed as

$$B_n(x) = \begin{cases} 1 - \dfrac{|x - x_n|}{\Delta}, & x_n - \Delta \le x \le x_n + \Delta \\ 0, & \text{else} \end{cases} \tag{13}$$

and has the Fourier transform

$$\tilde{B}_n(\beta_{xm}) = \Delta \operatorname{sinc}^2\left(\frac{\beta_{xm}\Delta}{2}\right) e^{-j\beta_{xm}x_n}. \tag{14}$$

The distribution of N triangle functions spans one unit cell of the Γ_1 plane, as illustrated in Fig. 3, and P triangle functions span one unit cell of the Γ_2 plane. The triangle functions are assumed to be evenly distributed and each has a half-width of Δ (this is not a necessary condition, but it is assumed for computational efficiency). It is observed that the basis function centered about $x = x'$ overlaps into the adjacent cell. This function is referred to as the continuity basis function, and ensures the continuity of the fields across the planes separating the unit cells.

The testing functions are chosen to be identical to the basis functions. By making use of (12), the k, nth term of the exterior impedance matrices $[Z^A]$ and $[Z^B]$ can be computed by the inner product

$$-\langle T_{zk}, E_{zn}^{\text{scat}} \rangle = \frac{k\eta}{b} \sum_{m=-\infty}^{\infty} \frac{1}{\beta_{ym}} \tilde{B}_k^*(\beta_{xm}) \tilde{B}_n(\beta_{xm}) = \frac{k\eta\,\Delta^2}{b} \sum_{m=-\infty}^{\infty} \frac{1}{\beta_{ym}} \operatorname{sinc}^4\left(\frac{\beta_{xm}\Delta}{2}\right) \cdot e^{-j\beta_{xm}(x_n - x_k)} \tag{15}$$

where k is the wave number, η is the characteristic wave impedance of the half-space, and β_{xm} and β_{ym} are defined

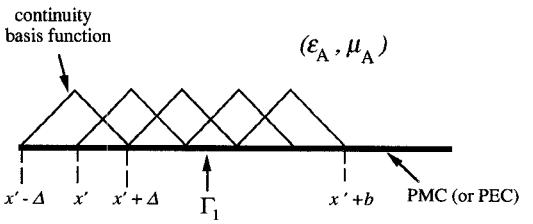

Fig. 3. Triangular basis functions spanning $\{x \in (x', x' + b)\}$ on Γ_1. The continuity basis function overlaps into the adjacent unit cell.

by (10) and (11). Equation (15) represents a TM-polarized incident wave. By duality, for a TE-polarized incident wave, the k, nth term of the exterior admittance matrices $[Y^A]$ or $[Y^B]$ can be computed from the inner product

$$-\langle T_{zk}, H_{zn}^{\text{scat}} \rangle = \frac{k\,\Delta^2}{\eta b} \sum_{m=-\infty}^{\infty} \frac{1}{\beta_{ym}} \operatorname{sinc}^4\left(\frac{\beta_{xm}\Delta}{2}\right) \cdot e^{-j\beta_{xm}(x_n - x_k)}. \tag{16}$$

These series converge rapidly, since the summand decays asymptotically as $1/m^5$. For this choice of basis functions, the summands of the series in (15) and (16) are dependent only upon the separation between the centers of the nth and the kth basis functions. Since the basis functions have been uniformly distributed, $(x_n - x_k) = \Delta(n - k)$. As a result, the entire admittance or impedance matrix can be constructed by only computing the elements of the first row of the matrix. This reduces the computational task from N^2 processes to N.

IV. Incorporating the Periodic Boundary Condition to Construct the Interior Impedance (Admittance) Matrix

The interior impedance (admittance) matrix is constructed by perturbing the interior region $(-d < y < 0)$ with each of the equivalent current basis functions, followed by the inner product of the induced aperture fields and a set of testing functions. Computation of the fields within the interior region using the FEM is the desired objective. However, the problem domain is not confined to a close region, as it was for the problems considered in [11], [12]. Rather, it spans the entire space $\{x \in [-\infty, +\infty]\}$. By taking advantage of the periodicity of the problem, a periodic boundary condition can be introduced that confines the problem domain to the unit cell. This is presented in this section.

Define the domain Ω' to be the domain of a single unit cell of the periodic structure

$$\{\Omega' : x \in (x', x' + b), y \in (-d, 0)\}. \tag{17}$$

The unit cell domain is bound by the contour Γ', which includes the surfaces of any nonpenetrable conducting material Γ_P, the Γ_1' and Γ_2' planes, and the periodic boundaries Γ_L and Γ_R, as illustrated in Fig. 4. It is noted that even though the boundaries Γ_L and Γ_R are assumed to be planar, this is not a necessary condition, and in fact, the side boundaries of the unit cell may be nonplanar.

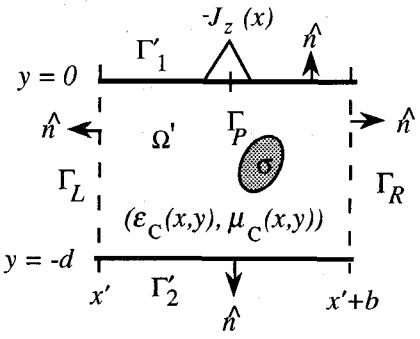

Fig. 4. The unit cell domain Ω', enclosed by the contour $\Gamma' = \Gamma'_1 + \Gamma'_2 + \Gamma_R + \Gamma_L + \Gamma_P$.

The fields within Ω' must satisfy the scalar Helmholtz wave equation

$$\nabla \cdot \frac{1}{\mu_r} \nabla\psi + \epsilon_r k_o^2 \psi = 0: \ \Omega' \tag{18}$$

where $\psi = E_z^{\text{tot}}$ for TM-polarized fields, with a dual expression applicable for TE-polarized fields. In the above expression, it is assumed that ϵ_r and μ_r have a spatial variation. Following the Galerkin method, the inner product (defined over the domain Ω') of (18) with a testing function Φ results in the expression

$$\iint_{\Omega'} \left[\Phi^* \nabla \cdot \frac{1}{\mu_r} \nabla\psi + \epsilon_r k_o^2 \Phi^* \psi \right] d\Omega' = 0. \tag{19}$$

The unit cell domain Ω' is then partitioned into N_e element domains Ω_e, and within each element domain, $\psi(\text{span } \Omega_e) = \psi_e$ and $\Phi(\text{span } \Omega_e) = \Phi_e$. As a result, (19) is expressed as a superposition of inner products within all the element domains Ω_e as

$$\sum_{e=1}^{N_e} \int_{\Omega_e} \left[\Phi_e^* \nabla \cdot \frac{1}{\mu_r} \nabla\psi_e + \epsilon_r k_o^2 \Phi_e^* \psi_e \right] d\Omega_e = 0. \tag{20}$$

Implementing the first form of Green's theorem leads to

$$\sum_{e=1}^{N_e} \left\{ \iint_{\Omega_e} \left[\frac{1}{\mu_r} \nabla\Phi_e^* \cdot \nabla\psi_e - \epsilon_r k_o^2 \Phi_e^* \psi_e \right] d\Omega_e - \int_{\Gamma_e} \frac{1}{\mu_r} \Phi_e^* \frac{\partial \psi_e}{\partial n} dl \right\} = 0 \tag{21}$$

where Γ_e is the contour enclosing the element domain Ω_e and n is along the direction of the outward normal at position l on Γ_e. Equation (21) is the discretized form of the weak form equation.

To this point, the field and the testing functions have been assumed to be arbitrary. However, for a valid solution of (21) both functions must belong to the functional space

$$\Lambda = \{\psi | \psi \in C^0; \ \ \psi(x + mb, y) = \psi(x, y) e^{jk_x mb}. \tag{22}$$

Due to the periodic nature of the source, the functional space is assumed to be composed of fields that have periodic distributions along the x-direction with a cell-to-cell phase shift of $e^{jk_x b}$, as specified by (4). However, from Floquet's theorem, all observable quantities have this phase shift. Therefore, the dual field is also periodic and from Maxwell's curl equation it can be stated that

$$\hat{n} \times \nabla\psi(x' + mb, y) = \hat{n} \times \nabla\psi(x', y) e^{jk_x mb}. \tag{23}$$

Maxwell's equations require that the tangential components of the electric and magnetic fields must be continuous across all boundaries. The scalar ψ represents the tangential component of the electric (or magnetic) field and is continuous across all boundaries from (22). The continuity of the tangential component of the electric (or magnetic) field is enforced in a weak sense by setting the line integral appearing in (21) to zero when Γ_e is a boundary shared between two element domains. Nonshared boundaries lie on the boundary Γ', which encloses the unit cell domain Ω'. As a result, (21) can be expressed as

$$\sum_{e=1}^{N_e} \left\{ \iint_{\Omega_e} \left[\frac{1}{\mu_r} \nabla\Phi_e^* \cdot \nabla\psi_e - \epsilon_r k_o^2 \Phi_e^* \psi_e \right] d\Omega_e \right\} - \sum_{b=1}^{N_b} \int_{\Gamma'} \frac{1}{\mu_r} \Phi_b^* \frac{\partial \psi_b}{\partial n} dl = 0 \tag{24}$$

where $\psi_b \subset \{\psi_e\}$ and $\Phi_b \subset \{\Phi_e\}$, and N_b is the number of element domains with edges on Γ'. For TM-polarized fields, the Dirichlet boundary condition $\psi = 0$ is enforced on the surface of a PEC, and the Neumann boundary condition $\partial\psi/\partial n = 0$ is satisfied in a weak sense on a PMC. For TE-polarized fields, a Neumann boundary condition is satisfied in a weak sense on the surface of a PEC. Therefore, on the boundaries Γ'_1 and Γ'_2, the contribution of the integral is zero, except in the presence of the equivalent current source, where

$$\partial\psi/\partial n = j\omega\mu J_z \ \ (\text{or } \partial\psi/\partial n = j\omega\epsilon M_z) \tag{25}$$

for TM (or TE) polarization.

It still remains to evaluate the contour integration over the periodic boundaries Γ_L and Γ_R. The periodic boundaries which truncate the problem domain to a single unit cell can be thought of as boundaries separating adjacent unit cells. However, since the electric and magnetic fields must be continuous across these boundaries, the contribution of the line integral over Γ_L and Γ_R must be zero. This can be shown explicitly by exploiting the periodic nature of the fields.

The line integral over Γ_L and Γ_R is expressed as

$$\int_{\Gamma_L} \frac{1}{\mu_r} \Phi^* \hat{n} \times \nabla\psi \, dl_L + \int_{\Gamma_R} \frac{1}{\mu_r} \Phi^* \hat{n} \times \nabla\psi \, dl_R \tag{26}$$

where $\hat{n}$ is the outward normal on Γ_L and Γ_R. Therefore, from (22) and (23), respectively, it can be stated that

$$\Phi^*(x' + b, y)|_{\Gamma_R} = \Phi^*(x', y) e^{-jk_x b}|_{\Gamma_L} \tag{27}$$

and

$$\hat{n} \times \nabla\psi(x' + b, y)|_{\Gamma_R} = \hat{n} \times \nabla\psi(x' + b, y) e^{jk_x b}|_{\Gamma_L}. \tag{28}$$

Inserting the expressions in (27) and (28) into (26) and choosing the appropriate normal vectors, this results in a natural boundary condition

$$\int_{\Gamma_L} \frac{1}{\mu_r} \Phi^* \hat{n} \times \nabla\psi \, dl_L + \int_{\Gamma_R} \frac{1}{\mu_r} \Phi^* \hat{n} \times \nabla\psi \, dl_R \equiv 0. \tag{29}$$

Physically, (29) implies that the electric and magnetic fields are continuous across the periodic boundaries from unit cell to unit cell. It also implies that the total time-average power leaving the unit cell along the periodic boundaries is zero. Furthermore, it satisfies the periodic boundary condition of the electric and magnetic fields in a weak sense. However, since ψ must satisfy the periodic boundary condition in a strict sense, it is still necessary to enforce (27) and the periodic condition in (22) as Dirichlet boundary conditions in (24).

The fields within each element domain are then expanded into trial functions weighted by unknown coefficients, with the simplest being first-order nodal elements (linear interpolate functions), where

$$\Phi_e = \sum_{i=1}^{n} v_{e_i} \lambda_{e_i} \quad \text{and} \quad \psi_e = \sum_{i=1}^{n} u_{e_i} \lambda_{e_i}. \tag{30}$$

Employing a global numbering scheme by enforcing the continuity of the fields across shared boundaries, (25) is expressed as a linear operator

$$(v^i, v^L, v^R)^H \begin{pmatrix} A^{ii} & A^{iL} & A^{iR} \\ A^{Li} & A^{LL} & 0 \\ A^{Ri} & 0 & A^{RR} \end{pmatrix} \begin{pmatrix} u^i \\ u^L \\ u^R \end{pmatrix} - (v^i, v^L, v^R)^H \begin{pmatrix} J_z^i \\ J_z^L \\ J_z^R \end{pmatrix} = 0 \tag{31}$$

where u^i is the vector of constant coefficients weighting the interior nodal elements (including Γ_1 and Γ_2), $(v^i)^H$ is the transpose conjugate of v^i, and u^L and u^R are the vectors of the constant weighting coefficients of the nodes lying on Γ_L and Γ_R, respectively. From the periodic boundary conditions,

$$u^R = u^L e^{jk_x b} \tag{32}$$

and

$$(v^R)^H = (v^L)^H e^{-jk_x b}. \tag{33}$$

Equations (32) and (33) are then enforced in a strict sense in (31).

The solution of the weak form equation is then found by evaluating the first variation of the linear functional with respect to $\{v\}$ at a stationary point. This results in the sparse linear system of equations:

$$\begin{pmatrix} A^{ii} & A^{iL} + A^{iR} e^{+jk_x b} \\ A^{Li} + A^{Ri} e^{-jk_x b} & A^{LL} + A^{RR} \end{pmatrix} \begin{pmatrix} u^i \\ u^L \end{pmatrix} = \begin{pmatrix} J_z^i \\ J_z^L + J_z^R e^{-jk_x b} \end{pmatrix}. \tag{34}$$

On the right-hand side of this expression, J_z^i is a vector computed via the contour integral in (25) and is only nonzero in the planes Γ_1' and Γ_2' when the edge of an interior nodal element, corresponding to node $(v^i)^H$, overlaps the support of the equivalent current basis function. A similar statement can be made for J_z^L and J_z^R.

Equation (34) is a sparse linear system of equations. If the material medium within Ω is lossless, then the sparse matrix is Hermitian. Exploiting this property leads to a savings in computational time and storage, and also results in a more stable factorization of the matrix. If the material medium is lossy, the matrix is nonHermitian, however, savings in computational time and storage can still be realized by taking advantage of the symmetry of the large matrix block A^{ii}.

The equivalent basis function set within a unit cell is given by (13) and is illustrated in Fig. 3. The interior region is perturbed by each basis function, and the fields within a single unit cell are solved using (34). Since only the right-hand side is changed by the excitation, the sparse matrix may be computed and factored once. Subsequently, the fields within Ω' can be derived for each equivalent current basis function, and the impedance matrix $[Z^C]$ (or admittance matrix $[Y^C]$) can be constructed.

V. Numerical Results

The previous algorithm has been incorporated into a computer program for the Convex C240 computer. First-order nodal elements were used to model the scalar electric or magnetic field within the cavity region. Typically, 400 elements per λ^2 were used. The sparse linear system of equations representing the interior problem was solved using the YSMP package [15], which is based on the minimum-degree ordering algorithm. It is noted that by incorporating the periodic boundary condition into (31), additional coupling between elements is encountered. However, this had little effect on the time required to factorize the matrix. The equivalent current basis function set that was used is the triangular basis set in (13). Approximately eight basis functions per λ over the exterior surfaces of a unit cell are necessary for convergence to an accurate solution. The aperture impedance (or admittance) matrices are then constructed, resulting in a small dense linear system of equations.

Once the approximate equivalent currents are computed, the time-averaged reflected and transmitted powers normal to the plane of the grating of the mth harmonic are computed. The accuracy of the approximate solution can be verified by the conservation of power. This is a necessary condition, but not sufficient. Nevertheless, once the code is validated, it provides confidence in the ap-

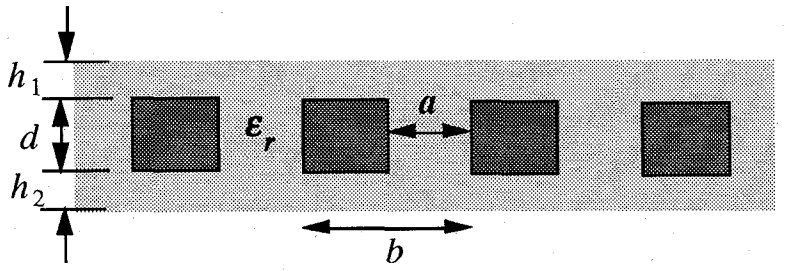

Fig. 5. Thick PEC grating embedded in a dielectric slab.

proximate solution when treating a noncanonical problem.

For validation purposes, the case of the scattering by a thick strip grating is first studied. Consider the thick PEC grating illustrated in Fig. 5. The grating is assumed to be embedded in a dielectric slab, with a thickness greater than that of the PEC grating. The material medium above and below the slab is assumed to be free space. Initially, the relative permittivity of the dielectric slab is chosen to be one, such that the PEC grating is effectively situated in free space. This problem was also studied by Gedney and Mitta in [12]. Fig. 6 illustrates the normalized reflected powers of the propagating harmonics versus frequency (represented as b/λ_o) when the PEC grating is illuminated by a normally incident TM-polarized plane wave. (The normalized power is the time-averaged power in the normal direction of the mth harmonic normalized by the normal time-averaged power of the incident field.) The grating has a unit cell width b and a separation of $a = 0.6\ b$ between the PEC cylinders of thickness $d = 0.4\ b$. The Γ_1 and Γ_2 planes are placed a distance of $0.1\ b$ above and below the PEC surface. In the problem, results were computed using the current method and were compared with those computed via the method presented in [12], which places the Γ_1 and Γ_2 on the surface of the PEC conductors. These results compare extremely well for all the propagating harmonics. The results were also verified for other angles of incidence and for the TE-polarized case, establishing confidence in the method and the computer code.

Next, the case in which the thick PEC grating is situated in a homogeneous dielectric slab is considered. For the case when $\epsilon_r = 2.56$, Figs. 7 and 8 illustrate the normalized reflected and transmitted powers, respectively, when the grating is illuminated by a normally incident TM-polarized plane wave. The dimensions of the conductors are the same as those considered in the previous case. The grating is almost purely reflecting at low frequencies (i.e., when the unit cell width is small compared to a wavelength). However, due to the presence of the dielectric slab, the surface becomes highly transmitting at a frequency well below the first Wood's anomaly, which occurs when $b/\lambda_o = 1.0$. Since the $TM_{0,0}$ mode does not propagate, if the slab is removed, this transition will take place at the Wood's anomaly, as is observed in Fig. 6.

The problem illustrated in Fig. 5 can also be considered

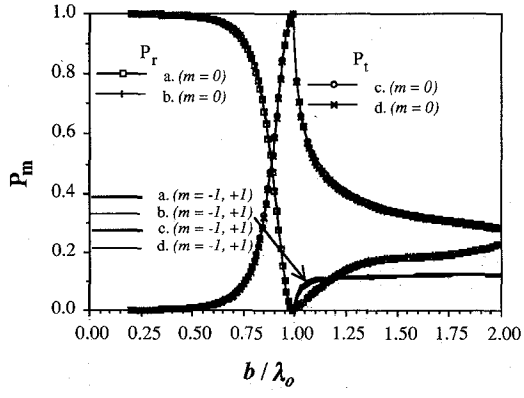

Fig. 6. Normalized power due to a TM-polarized incident plane wave on a thick grating ($\phi' = 90°$, $\epsilon_r = 1.0$, $d = 0.4\ b$, $a = 0.6\ b$, $h_1 = h_2 = 0.1\ b$). Case a: P_{rm} computed via FEM/MoM method outlined in [12]; Case b: P_{rm} computed via present method; Case c: P_{tm} computed via method outlined in [12]; Case d: P_{tm} computed via present method.

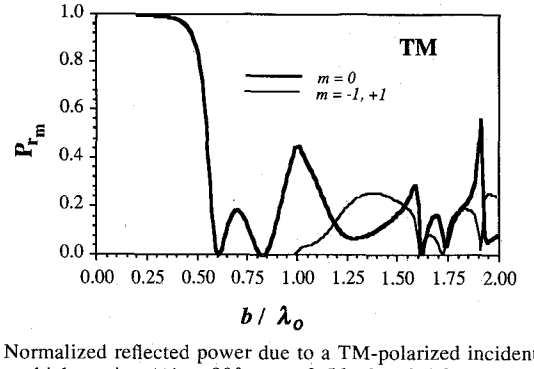

Fig. 7. Normalized reflected power due to a TM-polarized incident plane wave on a thick grating ($\phi' = 90°$, $\epsilon_r = 2.56$, $d = 0.4\ b$, $a = 0.6\ b$, $h_1 = h_2 = 0.1\ b$).

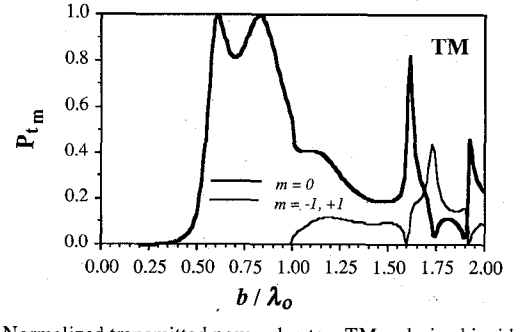

Fig. 8. Normalized transmitted power due to a TM-polarized incident plane wave on a thick grating ($\phi' = 90°$, $\epsilon_r = 2.56$, $d = 0.4\ b$, $a = 0.6\ b$, $h_1 = h_2 = 0.1\ b$).

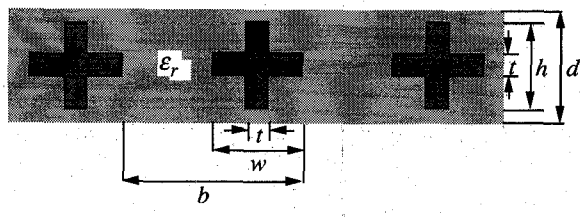

Fig. 9. PEC cross grating imbedded in a homogeneous dielectric slab.

using the method presented in [12], assuming that the dielectric slab is homogeneous above and below the conductors. In order to treat this problem, the Green's function can be readily expressed in the spectral domain. However, special attention must be given to the branch-point singularities that are inherent to this Green's function when performing the numerical integration. The advantage of treating the problem using the current method is that the exterior problem can be assumed to be a homogeneous half-space. The Green's function is easily handled here and is more computationally efficient. Furthermore, the case of an inhomogeneous slab above or below the conductors can easily be studied using the current method.

With the use of the finite elements, the conductors can be of arbitrary cross section such as the grating in Fig. 9, which is composed of PEC crosses imbedded in a homogeneous dielectric slab. It is assumed that the slab has a thickness $d = 0.5\ b$, and a relative permittivity $\epsilon_r = 2.56$. The crosses have a height of $0.5\ b$, and a width of $0.5\ b$, and the thickness of the arms is assumed to be $0.1\ b$. Figs. 10 and 11 illustrate the normalized reflected powers of the propagating harmonics versus frequency when the cross grating is illuminated by TM- and TE-polarized plane waves, respectively, with angle of incidence $\phi' = 60°$.

The second class of problems considered are dielectric gratings that are composed entirely of perfect dielectrics. Consider the grating illustrated in Fig. 12, which consists of square dielectric rods with permittivity ϵ_2 periodically distributed within a planar dielectric slab of permittivity ϵ_1. The dielectric slab is assumed to be homogeneous with permittivity $\epsilon_1 = 2.0\ \epsilon_0$. The normalized transmitted power versus frequency (represented as b/λ_o) of this grating illuminated by normally incident TM- and TM-polarized plane waves is illustrated in Figs. 13 and 14, respectively. Initially consider case a., when the dielectric rods have permittivities of $\epsilon_2 = 2.4\ \epsilon_o$. At low frequencies, the response appears to be that of a homogeneous slab, and the grating is highly transmitting. However, due to the periodic distribution of the dielectric rods, the grating becomes highly reflective within a small band of frequencies. Due to the low contrast between the rods and the slab, the bandwidth of these notches in the transmitted power is extremely small, as illustrated in Figs. 13 and 14. Therefore, this grating is highly frequency-selective. Increasing the relative permittivity of the dielectric rods results in the broadening of the bandwidth of the notches in the transmitted power, as demonstrated by case b., when $\epsilon_2 = 4.0\ \epsilon_o$. Here, it is observed that the bandwidths of the regions of high reflectivity have broadened. Furthermore, by increasing the contrast between the two dielectrics, the frequencies at which the surface becomes almost totally reflecting are lowered, and additional bands are introduced before the first resonance of the periodic structure.

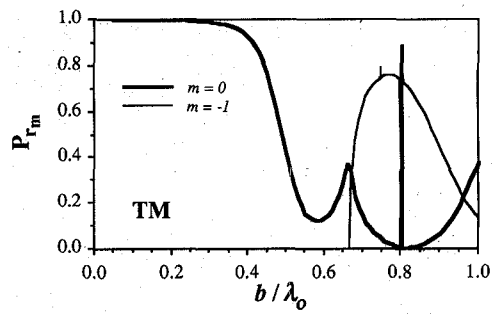

Fig. 10. Normalized reflected power due to a cross grating illuminated by a TM-polarized plane waves ($\epsilon_r = 2.56$, $d = 0.75\ b$, $t = 0.1\ b$, $w = 0.5\ b$, $h = 0.5\ b$, $\phi' = 60°$).

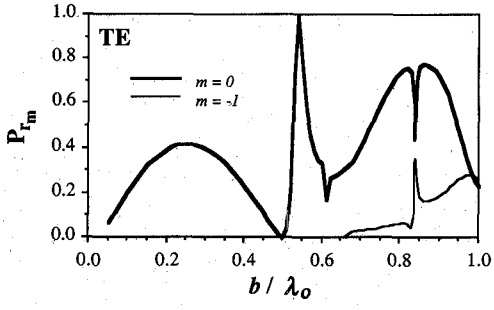

Fig. 11. Normalized reflected power due to a cross grating illuminated by a TE-polarized plane wave ($\epsilon_r = 2.56$, $d = 0.75\ b$, $t = 0.1\ b$, $w = 0.5\ b$, $h = 0.5\ b$, $\phi' = 60°$).

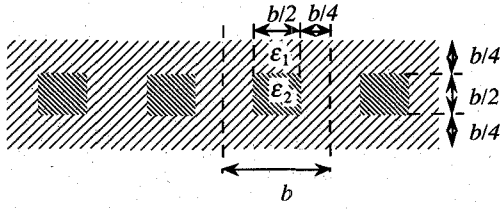

Fig. 12. Dielectric slab grating.

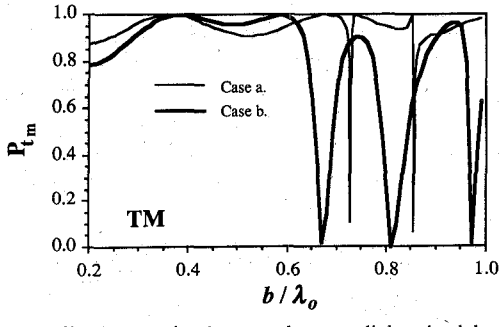

Fig. 13. Normalized transmitted power due to a dielectric slab grating illuminated by a TM-polarized plane wave ($\epsilon_1 = 2.0\ \epsilon_o$, $\phi' = 90°$). Case a: $\epsilon_2 = 2.4\ \epsilon_o$. Case b: $\epsilon_2 = 4.0\ \epsilon_o$.

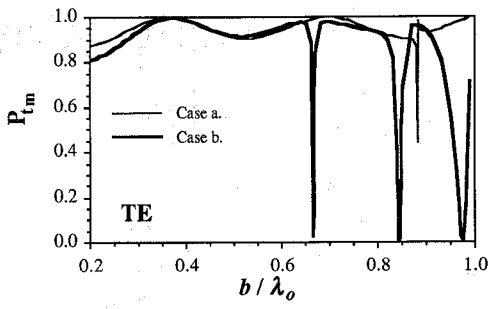

Fig. 14. Normalized transmitted power due to a dielectric slab grating illuminated by a TE-polarized plane wave ($\epsilon_1 = 2.0\ \epsilon_o$, $\epsilon' = 90°$). Case a: $\epsilon_2 = 2.4\ \epsilon_o$. Case b: $\epsilon_2 = 4.0\ \epsilon_o$.

VI. Summary

This paper has focused on the numerical anlysis of the diffraction of electromagnetic plane waves by arbitrary gratings. The gratings are assumed to be composed of inhomogeneous isotropic dielectric or magnetic materials, which may have conducting materials periodically distributed within them. The numerical method employed for the analysis was the combined FEM/MoM solution, which is based on the generalized network formulation. Due to the properties of the grating, the interior cavity region is infinite in extent. However, with the introduction of a periodic boundary condition, the interior problem domain was reduced to that of a single unit cell. The advantage of this formulation is that the sparsity of the interior finite element matrix is preserved, and with the use of direct methods of solution, the construction of the interior impedance (admittance) matrices can be performed quite efficiently.

A number of examples of gratings composed of piecewise homogeneous materials were presented in order to validate the method and to illustrate the types of problems that can be treated with this method. However, due to the robustness of the combined FEM/MoM solution, many other classes of problems may be considered. For example, problems for which the profile of the material constants and/or the surface profile of the grating are modulated is of great interest and can be studied using this method. Furthermore, gratings with higher degrees of inhomogeneity can also be studied with little additional computational cost.

References

[1] R. Petit, Ed., *Electromagnetic Theory of Gratings*. New York: Springer-Verlag, 1980.

[2] T. Gaylord and M. Moharam, "Analysis and applications of optical diffraction by gratings," *Proc. IEEE*, vol. 73, pp. 894–937, May 1985.

[3] M. Moharam and T. Gaylord, "Rigorous coupled-wave analysis of planar-grating diffraction," *J. Optical Society of America*, vol. 71, pp. 811–818, July 1981.

[4] R. S. Chu and J. A. Kong, "Modal theory of spatially periodic media," *IEEE Trans. Microwave Theory Tech.*, vol. MTT-25, pp. 18–24, Jan. 1977.

[5] M. Neviere, M. Cadilhac, and R. Petit, "Contribution a l'etude theorique de l'influence d'une couch dielectrique sur l'efficacite d'un reseau infiniment conducteur," *Optics Communications*, vol. 6, pp. 34–37, Sept. 1972.

[6] R. C. Hall, R. Mittra, and K. M. Mitzner, "Scattering from finite thickness resistive strip gratings," *IEEE Trans. Antennas Propagat.*, vol. 36, pp. 504–510, Apr. 1988.

[7] R. E. Jorgenson and R. Mittra, "Oblique scattering from lossy strip structures with one-dimensional periodicity," *IEEE Trans. Antennas Propagat.*, vol. 38, pp. 212–219, Feb. 1990.

[8] J. P. Montgomery, "Scattering by an infinite array of multiple parallel strips," *IEEE Trans. Antennas Propagat.*, vol. AP-27, pp. 798–807, Nov. 1979.

[9] K. Kobayashi and K. Miura, "Diffraction of a plane wave by a thick strip grating," *IEEE Trans. Antennas Propagat.*, vol. 37, pp. 459–470, Apr. 1989.

[10] M. Moaveni, "Analysis of transmission gratings by the method of finite elements," *Proc. IEE*, vol. 126, pp. 35–40, Jan. 1979.

[11] M. Moaveni, "Plane-wave scattering by gratings of conducting cylinders embedded in an inhomogeneous and lossy dielectric," *J. Optical Society of America*, vol. 5, pp. 834–842, June 1988.

[12] S. Gedney and R. Mittra, "Analysis of the electromagnetic scattering by thick gratings using a combined FEM/MoM solution," *IEEE Trans. Antennas Propagat.*, vol. 39, pp. 1605–1614, Nov. 1991.

[13] R. F. Harrington and J. R. Mautz, "A generalized network formulation for aperture problems," *IEEE Trans. Antennas Propagat.*, vol. AP-24, pp. 870–873, Nov. 1976.

[14] A. Papoulis, *The Fourier Integral and Its Application*. New York, NY: McGraw-Hill, 1962.

[15] S. C. Eisenstat, M. C. Gursky, M. H. Schultz, and A. H. Sherman, "Yale sparse matrix package. 1: The symmetric codes," *Inter. J. Numerical Methods in Engineering*, vol. 18, pp. 1145–1151, 1982.

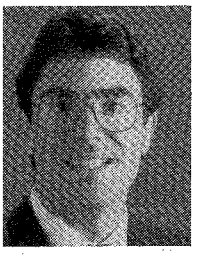

Stephen D. Gedney (S'84–M'90) was born in Poughkeepsie, NY in 1962. He received the B.Eng. honors-electrical degree from McGill University, Montreal, PQ, in 1985, and the M.S. and Ph.D. degrees from the University of Illinois, Urbana-Champaign, in 1987 and 1991.

From 1985 to 1987 he worked with the U.S. Army Corps of Engineers in Champaign, IL, where his research was in the area of EMP simulation, hardening and compatibility. From 1987 to 1991, he was a graduate Research Assistant and Teaching Assistant at the University of Illinois. For the 1989-1990 academic year, he was the recipient of the Harold L. Oleson award for excellence in teaching by a graduate student. Currently, he is an Assistant Professor at the University of Kentucky. His current research interests include the electromagnetic scattering by complex bodies, optical and microwave diffraction gratings, and numerical methods which exploit multiprocessor computers.

Jin-Fa Lee (S'85–M'85–S'86–M'88) for a photograph and biography see this issue, p. 352.

Raj Mittra (S'54–M'57–SM'69–F'71), for a photograph and biography, see this issue, p. 352.